Micromagnetics: Finite Element Approach

Since the early 1970s finite element modeling has become increasingly important in such different areas as continuum mechanics, electromagnetic field computation, and computational fluid dynamics. The integration of computer-aided design, finite element processing, and postprocessing methods for visualization of the numerical results makes finite element software a highly flexible tool in industrial research and development. The possibility of solving partial differential equations on irregular-shaped problem domains and of adjusting the spatial resolution using adaptive mesh refinement techniques are among the advantages of the finite element method. The use of the finite element method in micromagnetic simulations allows the realistic physical microstructures to be taken into account, which is a prerequisite for the quantitative prediction of the magnetic properties of thin film recording media or permanent magnets. Finite element models of the grain structure are obtained from a Voronoi construction and subsequent meshing of the polyhedral regions. Finite element micromagnetic codes have been developed for the calculation of equilibrium states and the simulation of magnetization reversal dynamics. In either case short-range exchange and long-range magnetostatic interactions between the grains considerably influence the magnetic properties. The numerical evaluation of the magnetostatic interaction field makes use of well-established techniques of magnetostatic field calculation based on the finite element or the boundary element method.

Numerical micromagnetics at a subgrain level involves two different length scales which may vary by orders of magnitude. The characteristic magnetic length scale on which the magnetization changes its direction, is given by the exchange length in soft magnetic materials and the domain wall width in hard magnetic materials. For a wide range of magnetic materials, this characteristic length scale is in the order of 5 nm which may be either comparable or significantly smaller than the grain size. Adaptive refinement and coarsening of the finite element mesh enables accurate solutions to be found of the magnetization distribution at a subgrain level.

1. Finite Element Models of Granular Magnets

The simulation of grain growth using a Voronoi construction (Preparata 1985) yields a realistic microstructure for a permanent magnet. Starting from randomly located seed points, the grains are assumed to grow with constant velocity in each direction. Then the grains are given by the Voronoi cells surrounding each point. The Voronoi cell of seed point i contains all points in space which are closer to seed point i than to any other seed point. In order to avoid strongly irregular-shaped grains, it is possible to divide the model magnet into cubic cells and to choose one seed point within each cell at random. An example is the grain structure of Fig. 1 which is used to simulate the magnetic properties of nanocomposite, permanent magnets. Different crystallographic orientations and different intrinsic magnetic properties are assigned to each grain. In addition, the grains may be separated by a narrow intergranular phase (Fischer and Kronmüller 1998). Once the polyhedral grain structure is obtained, the grains are further subdivided into finite elements. The magnetization is defined at the nodal points of the finite element mesh. Within each element the magnetization is interpolated by a polynomial function. Thus the magnetization $\mathbf{M}(\mathbf{r})$ may be evaluated everywhere within the model magnet, using the piecewise polynomial interpolation of the magnetization on the finite element mesh. Figure 2(a) illustrates the interpolation of the magnetization using a linear function on a triangular finite element. The magnetization on a point $\mathbf{r}$ within the element

$$\begin{aligned}\mathbf{M}(\mathbf{r}) &= (A_1\mathbf{M}(\mathbf{r}_1)+A_2\mathbf{M}(\mathbf{r}_2)+A_3\mathbf{M}(\mathbf{r}_3))/\\ &\quad (A_1+A_2+A_3)\\ &= (A_1/A)\mathbf{M}_1+(A_2/A)\mathbf{M}_2+(A_3/A)\mathbf{M}_3 \qquad (1)\end{aligned}$$

is the weighted average of the magnetization at the nodal points 1, 2, and 3. A denotes the total area of the element and A_i are the areas of the subtriangles (see Fig. 2). A similar interpolation scheme applies for tetrahedral elements in three dimensions. The functions $\varphi_i = A_i/A$ are called shape functions. The shape function $\varphi_i(\mathbf{r})$ equals one on the node i and is zero on all the other nodes of the element. The shape function $\varphi_i(\mathbf{r})$ satisfies the conditions

$$\varphi_i(\mathbf{x}_j) = \delta_{ij} \qquad (2)$$

where $\mathbf{r}_j$ denotes the cartesian coordinates of the nodes $j = 1,\ldots, n$. Figure 2(b) depicts the shape function φ_1. The finite element mesh is used to integrate the total magnetic Gibbs free energy over the magnet. The energy integral is then replaced by a sum over cells (triangles, tetrahedrons, hexahedrons, ...) and Eqn. (1) is applied to perform the integration of the energy over each cell.

Within the framework of micromagnetism (Brown 1963, Aharoni 1996), the magnitude of $\mathbf{M}$ is assumed to be a constant over the whole magnet, which depends only on the temperature

$$|\mathbf{M}| = M_s(T) \qquad (3)$$

The linear interpolation, Eqn. (1), does not preserve the magnitude of the magnetization within a finite element. However, the deviation of $|\mathbf{M}|$ from M_s within an element may be used as an error indicator for adaptive refinement schemes. Successive refinement of elements, where $|\mathbf{M}|$ deviates from M_s will

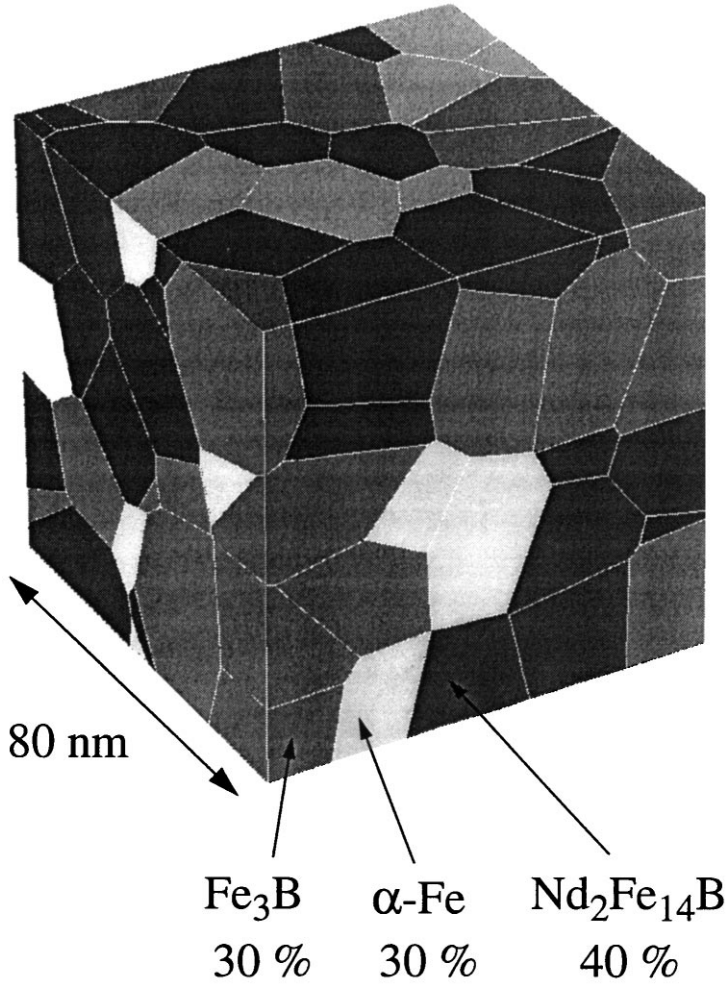

Figure 1
Finite element model of a nanocomposite permanent magnet obtained from a Voronoi construction. The plot gives the grain structure on the surface of a cubic magnet. The different colors refer to magnetically hard ($Nd_2Fe_{14}B$) and (α-Fe, Fe_3B) soft grains.

lead to a fine mesh in areas with large spatial variation of the magnetization direction. After several refinement steps the constraint, Eqn. (3), will be approximately fulfilled on the entire finite element mesh (see Sect. 5).

2. Total Magnetic Gibbs Free Energy and Effective Field

In numerical micromagnetics generally the following scheme is used in order to calculate a hysteresis loop. At first the model magnet is saturated by applying a high external field. The uniform magnetic state with magnetization pointing parallel to the field direction corresponds to a minimum of the total magnetic Gibbs free energy. The repeated minimization of the energy for decreasing and increasing applied field provides the hysteresis curve. A small change of the external fields alters the energy surface slightly and thus the system is not in equilibrium any more. Unless the change of the external field alters the curvature of the energy surface, the current position of the system will be close to a local minimum of the energy. If the local minimum vanishes as the curvature changes the system has to find its path towards the next local minimum. The Gilbert equation of motion (Gilbert 1955)

$$\frac{\partial \mathbf{M}}{\partial t} = -|\gamma|\,\mathbf{M}\times\mathbf{H}_{\text{eff}} + \frac{\alpha}{M_s}\mathbf{M}\times\frac{\partial \mathbf{M}}{\partial t} \qquad (4)$$

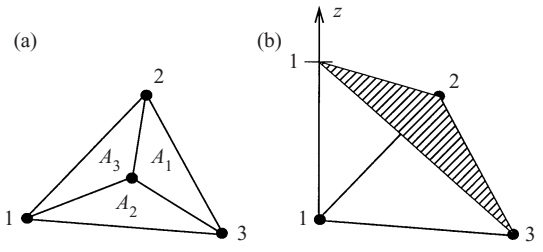

Figure 2
(a) Linear interpolation of the magnetization within a finite element. (b) The hatched area denotes the shape function of node 1, which equals one on node 1 and is zero on all the other nodes of the element.

is believed to describe the physical path the system follows towards equilibrium. The effective field $\mathbf{H}_{\text{eff}}$ which provides the torque acting on the magnetization is the negative functional derivative of the total magnetic Gibbs free energy, $\mu_0\mathbf{H}_{\text{eff}} = -\delta E/\delta\mathbf{M}$. The first term on the right hand side of Eqn. (4) describes the gyromagnetic precession, where γ is the gyromagnetic ratio of the free electron spin. The second term describes the dissipation of energy. It causes the magnetization to be become aligned parallel with the effective field as the system proceeds towards equilibrium. α is a dimensional damping parameter. Alternatively, numerical minimization methods may be used to compute the equilibrium states which considerably reduce the computation effort as compared to the numerical integration of the Gilbert equation.

Both static and dynamic micromagnetic finite element calculations start from the discretization of the total magnetic Gibbs free energy

$$E = \int \mathrm{d}V\{e_{\text{ex}}(\mathbf{r}) + e_{\text{K}}(\mathbf{r}) + e_{\text{m}}(\mathbf{r}) + e_{\text{z}}(\mathbf{r})\} \tag{5}$$

which is the integral over the sum of the exchange energy density, the magneto-crystalline anisotropy energy density, the magnetostatic energy density, and the Zeeman energy density. When $\mathbf{M}(\mathbf{r})$ is approximated by piecewise polynomial functions on the finite element mesh, the energy functional reduces to an energy function with the nodal values of the magnetization, $\mathbf{M}_i = (M_{x,i}, M_{y,i}, M_{z,i})$, as unknowns. The total energy may be written as

$$\begin{aligned} E &= E(\mathbf{M}(\mathbf{r})) = E(\mathbf{M}_1, \mathbf{M}_2, \ldots, \mathbf{M}_n) \\ &= E(M_{x,1}, M_{y,1}, M_{z,1}, M_{x,2}, M_{y,2}, M_{z,2}, \ldots, \\ &\quad M_{x,n}, M_{y,n}, M_{z,n}) \end{aligned} \tag{6}$$

where n is the total number of nodal points. The minimization of Eqn. (6) with respect to the $3n$ variables $M_{x,i}, M_{y,i}, M_{z,i}$ subject to the constraint $|\mathbf{M}_i| = M_{\text{s}}$ provides an equilibrium distribution of the magnetization. To satisfy the constraint, Eqn. (3), polar coordinates θ_i, ϕ_i for the magnetization at the node i may be introduced, such that $M_{x,i} = M_{\text{s}} \sin\theta_i \cos\phi_i$, $M_{y,i} = M_{\text{s}} \sin\theta_i \sin\phi_i$, and $M_{z,i} = M_{\text{s}} \cos\theta_i$. An alternative approach (Koehler 1997) is to normalize the magnetization in the discretized energy function, Eqn. (6), replacing $M_{x,i}, M_{y,i}, M_{z,i}$ by $M_{x,i}/|\mathbf{M}_i|, M_{y,i}/|\mathbf{M}_i|, M_{z,i}/|\mathbf{M}_i|$. In both cases, the minimization may be effectively performed using a conjugate gradient method (Gill *et al.* 1993). Conjugate gradient-based minimization techniques require the gradient of the energy to select the search directions. Using polar coordinates, the gradient of the energy can be expressed as

$$\begin{aligned} \frac{\partial E}{\partial \theta_i} &= \frac{\partial E}{\partial M_{x,i}}\frac{\partial M_{x,i}}{\partial \theta_i} + \frac{\partial E}{\partial M_{y,i}}\frac{\partial M_{y,i}}{\partial \theta_i} + \frac{\partial E}{\partial M_{z,i}}\frac{\partial M_{z,i}}{\partial \theta_i} \\ &= -V_i\mu_0\mathbf{H}_{\text{eff},i} \cdot \frac{\partial \mathbf{M}_i}{\partial \theta_i} \end{aligned} \tag{7}$$

$$\begin{aligned} \frac{\partial E}{\partial \phi_i} &= \frac{\partial E}{\partial M_{x,i}}\frac{\partial M_{x,i}}{\partial \phi_i} + \frac{\partial E}{\partial M_{y,i}}\frac{\partial M_{y,i}}{\partial \phi_i} + \frac{\partial E}{\partial M_{z,i}}\frac{\partial M_{z,i}}{\partial \phi_i} \\ &= -V_i\mu_0\mathbf{H}_{\text{eff},i} \cdot \frac{\partial \mathbf{M}_i}{\partial \phi_i} \end{aligned} \tag{8}$$

In Eqns. (7) and (8) the effective field $\mathbf{H}_{\text{eff}}$ has been introduced. The effective field at the nodal points of the finite element mesh can be calculated within the framework of the box method. The effective field at the nodal point i of the finite element mesh can be approximated by (Gardiner 1985)

$$\mu_0\mathbf{H}_{\text{eff},i} = -\left(\frac{\delta E}{\delta \mathbf{M}}\right)_i \approx -\frac{1}{V_i}\frac{\partial E}{\partial \mathbf{M}_i} \tag{9}$$

where V_i is the volume of a "box" surrounding the nodal point i. The following conditions hold for the box volumes

$$\sum_i V_i = \int \mathrm{d}V \quad \text{and} \quad V_i \cap V_j = 0 \quad \text{for } i \neq j. \tag{10}$$

3. *Magnetostatic Field Calculation*

Both static and dynamic micromagnetic calculations are required to evaluate the effective field at the nodal points of the finite element mesh. The effective field is the sum of the exchange field, the anisotropy field, the magnetostatic field, and the external field. The ex-

change field and the anisotropy field depend only locally on the magnetization or its spatial derivatives and thus may be directly calculated using Eqn. (9). The magnetostatic field depends on the magnetization distribution over the entire magnet. It arises from the nonzero divergence within the grains (''magnetic volume charges'') and the intersection of the magnetization with the grain surface (''magnetic surface charges'').

Numerical micromagnetics can make use of the well-established methods for the finite element calculation of magnetostatic fields (Silvester and Ferrari 1983). The magnetostatic field either is derived from a magnetic scalar or a magnetic vector potential. The finite element discretization of the corresponding partial differential equation leads to a system of linear equations. Owing to the local character of the equations the corresponding system matrix is symmetric and sparse. State of the art solution techniques for a sparse linear systems consist of a preconditioning step, followed by the iterative solution of the linear system using a conjugate gradient-based method. For a given finite element mesh the preconditioning of the system matrix has to be done only once, reducing the effort for the subsequent calculations of the magnetostatic field to about $n^{1.3}$, where n is the total number of grid points. Thus the use of the finite element method to treat the auxiliary problem of the magnetostatic field provides an alternative fast solution technique without any restriction on the geometry of the magnetic particles.

3.1 The Magnetostatic Boundary Value Problem

The magnetostatic contribution to the effective field is the negative gradient of the magnetic scalar potential. The magnetic scalar potential satisfies the Poisson equation

$$\nabla^2 U(\mathbf{r}) = \nabla \cdot \mathbf{M}(\mathbf{r}) \tag{11}$$

Outside the magnetic particle $\mathbf{M}$ equals zero and thus Eqn. (11) reduces to the Laplace equation. At the boundary of the magnet Γ the boundary conditions

$$U^{\text{int}} = U^{\text{ext}}, (\nabla U^{\text{int}} - \nabla U^{\text{ext}}) \cdot \mathbf{n} = \mathbf{M} \cdot \mathbf{n} \tag{12}$$

hold. Here $\mathbf{n}$ denotes the outward pointing normal unit vector on Γ. The magnetic scalar potential is regular at infinity

$$U \propto 1/\mathbf{r} \quad \text{for } \mathbf{r} \to \infty \tag{13}$$

The Galerkin method is applied to transfer the magnetostatic boundary value problem to a system of linear equations. The partial differential equation, Eqn. (11), is multiplied by test functions φ_i and integrated over the problem domain

$$\int_{\Omega_{\text{int}}} \mathrm{d}V \varphi_i \nabla^2 U(\mathbf{r}) + \int_{\Omega_{\text{ext}}} \mathrm{d}V \varphi_i \nabla^2 U(\mathbf{r}) = \int_{\Omega_{\text{int}}} \mathrm{d}V \varphi_i \nabla \cdot \mathbf{M}(\mathbf{r}) + \int_{\Omega_{\text{ext}}} \mathrm{d}V \varphi_i \nabla \cdot \mathbf{M}(\mathbf{r}) \tag{14}$$

Here Ω_{int} and Ω_{ext} denote the space within and outside the magnet, respectively. Integration by parts moves the second derivative of the potential and the first derivative of the magnetization vector to the test function

$$\int_{\Gamma} \mathrm{d}S \varphi_i (\nabla U^{\text{int}} - \nabla U^{\text{ext}}) \cdot \mathbf{n} - \int_{\Omega_{\text{int}} \cup \Omega_{\text{ext}}} \mathrm{d}V \nabla \varphi_i \nabla U = \int_{\Gamma} \mathrm{d}S \varphi_i \mathbf{M} \cdot \mathbf{n} - \int_{\Omega_{\text{int}}} \mathrm{d}V \nabla \varphi_i \cdot \mathbf{M} \tag{15}$$

Substituting the boundary condition, Eqn. (12), into Eqn. (15) the surface integrals cancel.

Within the framework of the Galerkin method, the shape functions φ_i, given by Eqn. (2), are used as test functions. Like the magnetization, the magnetic scalar potential is interpolated by a piecewise polynomial function over a finite element e

$$U(\mathbf{r}) = \sum_i \varphi_i^e(\mathbf{r}) U_i = \varphi_i^e(\mathbf{r}) U_i \tag{16}$$

where U_i denote the values of the magnetic scalar potential at the nodes of the element. Then the volume integrals in Eqn. (15) break into sums of integrals over the finite elements

$$\sum_e \int \mathrm{d}V \nabla \varphi_i \nabla \varphi_j^e U_j = \sum_e \int \mathrm{d}V \nabla \varphi_i \cdot \varphi_j^e \mathbf{M}_j \tag{17}$$

The summation over the contributions of the individual finite elements in Eqn. (17) leads the sparse, linear system of equations that gives the potential U_i at the nodes i of the finite element mesh.

3.2 The Open Boundary Problem

In order to impose the regularity condition Eqn. (13), the finite element mesh has to be extended over a large region outside the magnetic particles. As a rule of thumb the distance between the boundary of the external mesh and the particle should be at least five times the extension of the particle (Chen and Conrad 1997). Various other techniques have been proposed to reduce the size of the external mesh or to avoid a discretization of the exterior space. The use of asymp-

totic boundary conditions (Yang and Fredkin 1998) reduces the size of the external mesh compared to truncation. At the external boundary Robbin conditions are applied, which are derived from a series expansion of the solution of the Laplace equation for U outside the magnet and give the decay rate of the potential at a certain distance from the sample (Khebir *et al.* 1990).

A similar technique that considerably reduces the size of the external mesh is the use of space transformation to evaluate the integral over the exterior space in Eqn. (15). Among the various transformations proposed to treat the open boundary problem, the parallelepipedic shell transformation (Brunotte *et al.* 1992), which maps the external space into shells enclosing the parallelepipedic interior domain, has proved to be most suitable in micromagnetic calculations. The method can be easily incorporated into standard finite element programs transforming the derivatives of the nodal shape functions. This method was applied in static three-dimensional micromagnetic simulations of the magnetic properties of nanocrystalline permanent magnets (Schrefl and Fidler 1998, Fischer and Kronmüller 1998)

An alternative approach for treating the so-called open boundary problem is a hybrid finite element/boundary element method (Fredkin and Koehler 1990, Koehler 1997). The basic concept of this method is to split the magnetic scalar potential into $U = U_1 + U_2$, where the potential U_1 is assumed to solve a closed boundary value problem. Then the equations for U_2 can be derived from Eqns. (11) and (12), which hold for the total potential $U = U_1 + U_2$. The potential U_1 accounts for the divergence of the magnetization and U_2 is required to meet the boundary conditions at the surface of the particle. The latter also carries the magnetostatic interactions between distinct magnetic particles.

The potential U_1 can be computed from the closed boundary value problem

$$\nabla^2 U_1(\mathbf{r}) = \nabla \cdot \mathbf{M}(\mathbf{r}) \quad \text{for } \mathbf{r} \in \Omega_{\text{int}} \tag{18}$$

$$U_1 = 0 \quad \text{for } \mathbf{r} \in \Omega_{\text{ext}} \tag{19}$$

$$\nabla U_i \cdot \mathbf{n} = \mathbf{M} \cdot \mathbf{n} \quad \text{for } \mathbf{r} \in \Gamma \tag{20}$$

The potential U_1 is the solution of the Poisson equation within the magnetic particles and equals zero outside the magnets. At the surface of the magnets, natural boundary conditions hold. The potential U_2 satisfies the Laplace equation everywhere

$$\nabla^2 U(\mathbf{r}) = 0 \quad \text{for } \mathbf{r} \in \Omega_{\text{int}} \cup \Omega_{\text{ext}} \tag{21}$$

and shows a jump at the boundary of the magnetic particles

$$U_2^{\text{int}}(\mathbf{r}) - U_2^{\text{ext}}(\mathbf{r}) = U_1^{\text{int}}(\mathbf{r}), (\nabla U_2^{\text{int}} - \nabla U_2^{\text{ext}}) \cdot \mathbf{n} = 0 \quad \text{for } \mathbf{r} \in \Gamma \tag{22}$$

A standard finite element method may be used to solve Eqns. (18)–(22). Eqns. (21) and (22) define a double layer potential which is created by a dipole sheet with magnitude $U_1 \cdot U_2$ can be evaluated using the boundary element method. After discretization, the potential U_2 at the boundary nodes follows from a matrix vector multiplication $U_2 = \mathbf{B}\, U_1$, where $\mathbf{B}$ is a $m \times m$ matrix which relates the m boundary nodes with each other. Once U_2 at the boundary has been calculated, the values of U_2 within in the particles follow from Laplace's equation with Dirichlet boundary conditions, which again can be solved by a standard finite element technique. The matrix $\mathbf{B}$ depends only on the geometry and the finite element mesh and thus has to be computed only once for a given finite element mesh. Since the hybrid finite element boundary element method does not introduce any approximations, the method is accurate and effective. The use of the boundary element method easily treats the magnetostatic interactions between distinct magnetic particles and requires no mesh outside the magnetic particles. Süß and co-workers (Süß *et al.* 1999) applied the hybrid finite element/boundary element method, in order to simulate the effect of magnetostatic interactions on the reversal dynamics of magnetic nanoelements.

3.3 Static Micromagnetics Using a Magnetic Vector Potential

The use of a magnetic scalar potential in micromagnetic calculations, requires the solution of a system of linear equations associated with the magnetostatic boundary value problem, whenever the total magnetic Gibbs free energy or the effective field has to be evaluated. An alternative approach for treating the magnetostatic interactions is the use of a magnetic vector potential. Then micromagnetic problem can be reformulated as an algebraic minimization problem with the nodal values of the magnetization angles θ_i, ϕ_i, and the nodal values of the magnetic vector potential $\mathbf{A}$ as unknowns. The method applies an alternative function to express the magnetostatic energy.

Brown (1963) proposed an upper bound for the magnetostatic energy

$$\int \mathrm{d}V e_{\text{m}} \leqslant W(\mathbf{A}) = \frac{1}{2\mu_0} \int \mathrm{d}V (\nabla \times \mathbf{A} - \mu_0 \mathbf{M})^2 \tag{23}$$

If minimized with respect to $\mathbf{A}$, the functional $W(\mathbf{A})$ reduces to the magnetostatic energy of the magnetization distribution $\mathbf{M}(\mathbf{r})$. Thus it is possible to replace the magnetostatic energy in the total magnetic Gibbs free energy with $W(\mathbf{A})$ and treat $\mathbf{A}$ as an additional variable. The simultaneous minimization of the energy

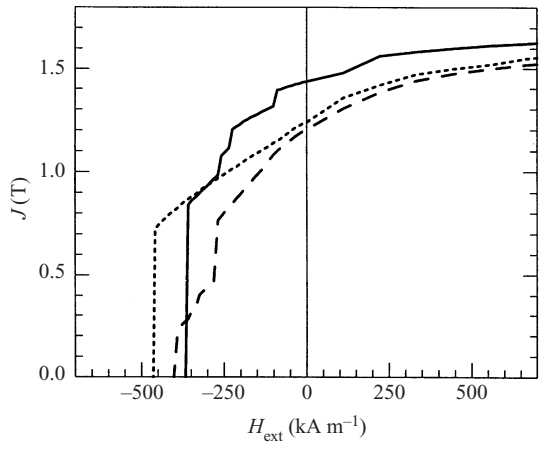

Figure 3
Numerically calculated demagnetization curves as a function of the mean grain size for the nanocomposite magnet of Fig. 1. ——, 10 nm; ·····, 20 nm; - - - -, 30 nm.

with respect to **M** and **A** provides the equilibrium configuration of the magnetization (Aharoni 1996). Again spherical coordinates can be introduced to satisfy the constraint (3). The integral on the right hand side of Eqn. (23) is an integration over the entire space and proper techniques to treat the open boundary problem have to be applied. The first variation of Eqn. (23) gives the unconstrained curl–curl equation for the magnetic vector potential which is the equation commonly solved in magnetostatic field calculations. Thus the use of a magnetic vector potential in numerical micromagnetics treats the magnetostatic field in the very same way as conventional finite element packages for magnetostatic field calculation (Demerdash and Wang 1990).

This method was applied to predict the theoretical limits for the remanence and the coercive field of nanocomposite permanent magnets (Schrefl and Fidler 1998). These magnets consist of a mixture of magnetically hard and soft phases. The complex, multiphase microstructure considerably influences the magnetic properties and thus has to be taken into account in micromagnetic models. Figure 3 gives the numerically calculated demagnetization curves for the $Nd_2Fe_{14}B$ magnet depicted in Fig. 1 as a function of the average grain diameter. Intergrain exchange interactions considerably enhance the remanence compared with the remanence of noninteracting, randomly oriented grains. Figure 4 presents the magnetization distribution in a slice plane for zero applied field and an average grain size of 20 nm. The magnetization remains parallel to the saturation direction within the soft magnetic grains, whereas it rotates towards the direction of the local anisotropy direction within the hard magnetic grains.

4. Dynamic Micromagnetics Using the Finite Element Method

Either a box scheme or the Galerkin method can be applied to discretize the Gilbert equation of motion, Eqn.(4), in space. The Gilbert equation (4) reduces to three ordinary differential equations for each node of the finite element mesh, using the box scheme, Eqn. (9), to approximate the effective field. The resulting system of *3n* ordinary differential equations describes the motion of the magnetic moments at the nodes of the finite element mesh. The system of ordinary differential equations is commonly solved using a predictor corrector method or a Runge Kutta method for mildly stiff differential equations. Small values of Gilbert damping constant α or complex microstructures will require a time step smaller than 10 fs, if an explicit scheme is used for the time integration. In this highly stiff regime backward difference schemes allow much larger time steps and considerably reduce the required CPU time.

An implicit time integration scheme can be derived, applying the Galerkin method directly to discretize the Gilbert equation (4). A backward difference method (Hindmarsh and Petzold 1995) is used for time integration of the resulting system of ordinary differential equations. Since the stiffness arises mainly from the exchange term, the magnetostatic field can be treated explicitly. During a time interval τ, the Gilbert equation is integrated with a fixed magnetostatic field using a higher order backward difference method. The magnetostatic field is updated after a time τ which is taken to be inversely proportional to the maximum torque $\max_i, |\mathbf{M}_i \times \mathbf{H}_{\mathrm{eff},i}|$ over the finite element mesh. The hybrid finite element/boundary element method is used to calculate the magnetostatic field. Figure 5 presents the flow chart of the semi-implicit time integration scheme. In highly stiff regimes the semi-implicit scheme requires less central processing unit (CPU) time as compared with a Runge–Kutta method, despite the need to solve a system of nonlinear equations at each time step.

A semi-implicit time integration scheme was applied to calculate the magnetization reversal dynamics of patterned Co elements, taking into account the small scale, granular structure of the thin films elements (Schrefl *et al.* 1999). Dynamic micromagnetic calculations using the finite element method and backward difference were originally introduced by Yang (Yang and Fredkin 1996) and applied to the study of magnetization reversal dynamics of interacting ellipsoidal particles (Yang and Fredkin 1998).

5. Adaptive Meshing

The finite element method effectively treats magnetization processes in samples with arbitrary geometries

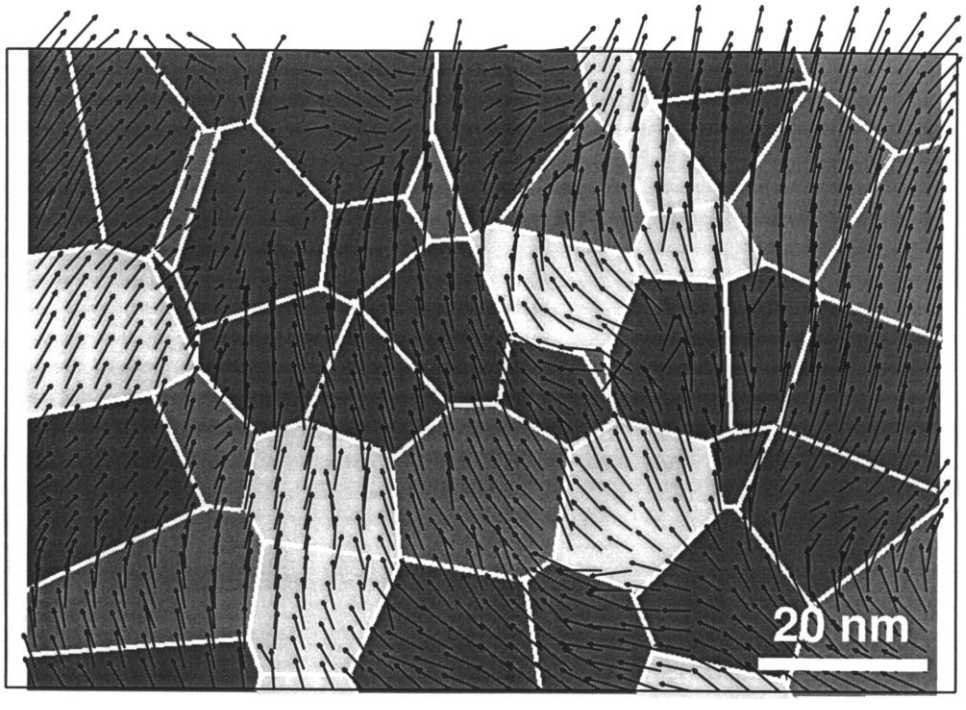

Figure 4
Magnetization distribution within a nanocomposite magnet for zero applied field. The arrows denote the direction of the magnetization in a slice plane parallel to the saturation direction. The mean grain size was 20 nm.

or irregular microstructures. Adaptive refinement schemes allow the magnetization distribution to be solved on a subgrain level, improving the accuracy of the solution while keeping the computational effort to a minimum. Finite element mesh refinement was applied in micromagnetic simulations of longitudinal thin film media (Tako *et al.* 1997), domain structures in soft magnetic thin films (Hertel and Kronmüller 1998), and domain wall motion in permanent magnets (Scholz *et al.* 1999).

6. *Refinement Indicators*

The discretization of the micromagnetic equations gives rise to two types of discretization error. One is associated with the evaluation of the exchange field, the other arises from the finite element computation of the magnetostatic field. Improvements in the micromagnetic resolution can be made by a uniform increase in the level of discretization. However, this places more computational modes in areas where the magnetization remains uniform. Ideally, it would be most efficient to place new nodes where the error is highest.

The aim of adaptive mesh refinement schemes is to obtain a uniform distribution of the discretization error over the finite element mesh (Penman and Grieve 1987). In order to decide where to refine the mesh, refinement indicators should give a good estimate of the local error. A second criterion for the selection of error estimators for adaptive meshing are the computational costs. Error estimators should be cheap to evaluate and thus error indicators derived from the current finite element solution on an element-by-element basis are preferred. Within the framework of classical micromagnetism the magnitude of the magnetization vector is assumed to be constant. This condition can only hold at the nodal points of the finite element mesh, using a linear interpolation of the magnetization on a finite element. Bagnérés-Viallix (Bagnérés-Viallix *et al.* 1991) proposed use of the deviations in the length of the magnetization vector from M_s in the center of an element as refinement indicator. The magnetization distribution of a one-dimensional domain wall can be calculated analytically. Thus the true discretization error of the finite element solution can be evaluated. Numerical investigations of one-dimensional mesh refinement showed that the error estimator based on the norm of the magnetization shows the very same functional dependence on the number of finite elements as the true error of the solution.

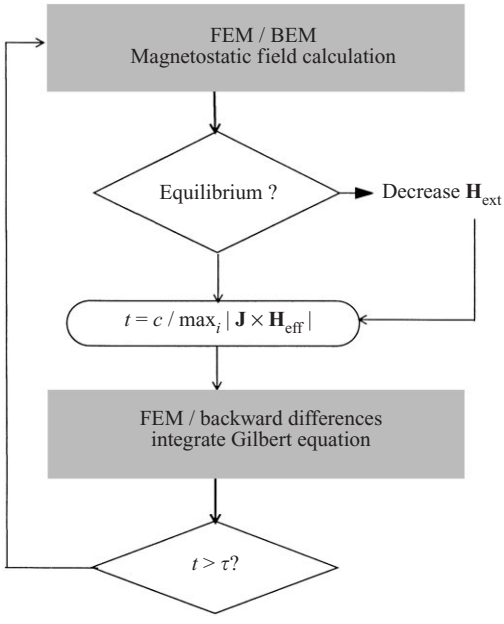

Figure 5
Flow chart of the semi-implicit time integration scheme used to solve the Gilbert equation of motion.

Refinement indicators that point out the exchange discretization error are usually based on the spatial variation of the magnetization (Hertel and Kronmüller 1998). They identify domain walls, vortices, or magnetic inhomogenities near edges and corners. In order to consider the discretization error associated with the magnetostatic field calculation, Tako *et al.* (1997) suggested a refinement indicator based on the divergence and curl of both the magnetization and magnetic field. Simulating the magnetization structure of two-dimensional magnetic nanoelements, Ridley *et al.* (1999) showed that this refinement indicator correctly identifies the regions where the true error in the computed magnetic field is high.

6.1 Finite Element Micromagnetics Using Adaptive Mesh Control

In longitudinal thin film media the granular microstructure significantly influences the remanent magnetization distribution. Tako (Tako *et al.* 1997) showed that adaptive refinement clearly improves both the efficiency and accuracy of the computations of magnetization patterns in thin film microstructures obtained form a Voronoi construction. A refinement indicator based on the spatial variation of both magnetization and magnetic field is used to point out elements in which refinement is necessary. Elements which show a refinement indicator greater than 20% of the maximum value over all elements are subdivided by regular division. The numerical results indicate a significant improvement in the calculated magnetization structure after refinement. The magnetization tends to form vortices which do not fully develop in the coarse grid. With further refinement the structure is allowed a lower energy state to be attained allowing a more complete development of the solenoidal structure. During the refinement process the total energy decreases by about 50% which clearly indicates the success of the refinement indicator.

Hertel and Kronmüller (1998) proposed an r-refinement scheme to resolve vortices in micromagnetic simulations of domain structures in soft magnetic, thin film elements. The discretization error is reduced by moving nodes of the finite element mesh towards regions where higher accuracy is needed. In micromagnetic simulations of domain structures in soft magnetic thin films, this was accomplished by shrinking the elements in regions with strong inhomogeneities. Thus, a high mesh density, which results in a high micromagnetic resolution, was obtained near vortices and domain walls, while keeping the number of elements constant.

In hard magnetic materials the magnetization is uniform within magnetic domains whereas it is highly nonuniform in domain walls, near nucleation sites, vortices, or grain boundaries. A coarse mesh may be sufficient in regions where the magnetization is almost uniform. Local mesh refinement near grain boundaries, domain walls, vortices, and nucleation sites significantly reduces the number of degrees of freedom. As domain walls can move because of external fields, the discretization has to be adjusted adaptively during the simulation. Scholz *et al.* (1999) presented an algorithm that adapts the finite element mesh to the solution of the Gilbert equation. Refinement of the tetrahedral mesh at the current wall position and coarsening within the bulk of the domains leads to a high density mesh that moves together with the wall. After each time step, error indicators based on the deviations of $|\mathbf{M}|$ from M_s are calculated for each element. If the maximum error indicator over all elements, η_{max}, exceeds a certain threshold the following refinement scheme is applied: Elements whose error indicators exceeds $0.1\eta_{max}$ are marked for refinement, whereas elements with an error indicator lower than $0.01\ \eta_{max}$ are marked for coarsening. Then, the finite element mesh is refined by subdividing elements, which are marked for refinement. Coarsening is effected by removing finite elements which have been created by an earlier refinement step (Bey 1995). Figure 6 shows the regions of fine mesh at the current wall position during the simulation of domain wall motion in thin $Nd_2Fe_{14}B$ specimens. The wall moves towards the boundary of a misoriented grain, where it remains

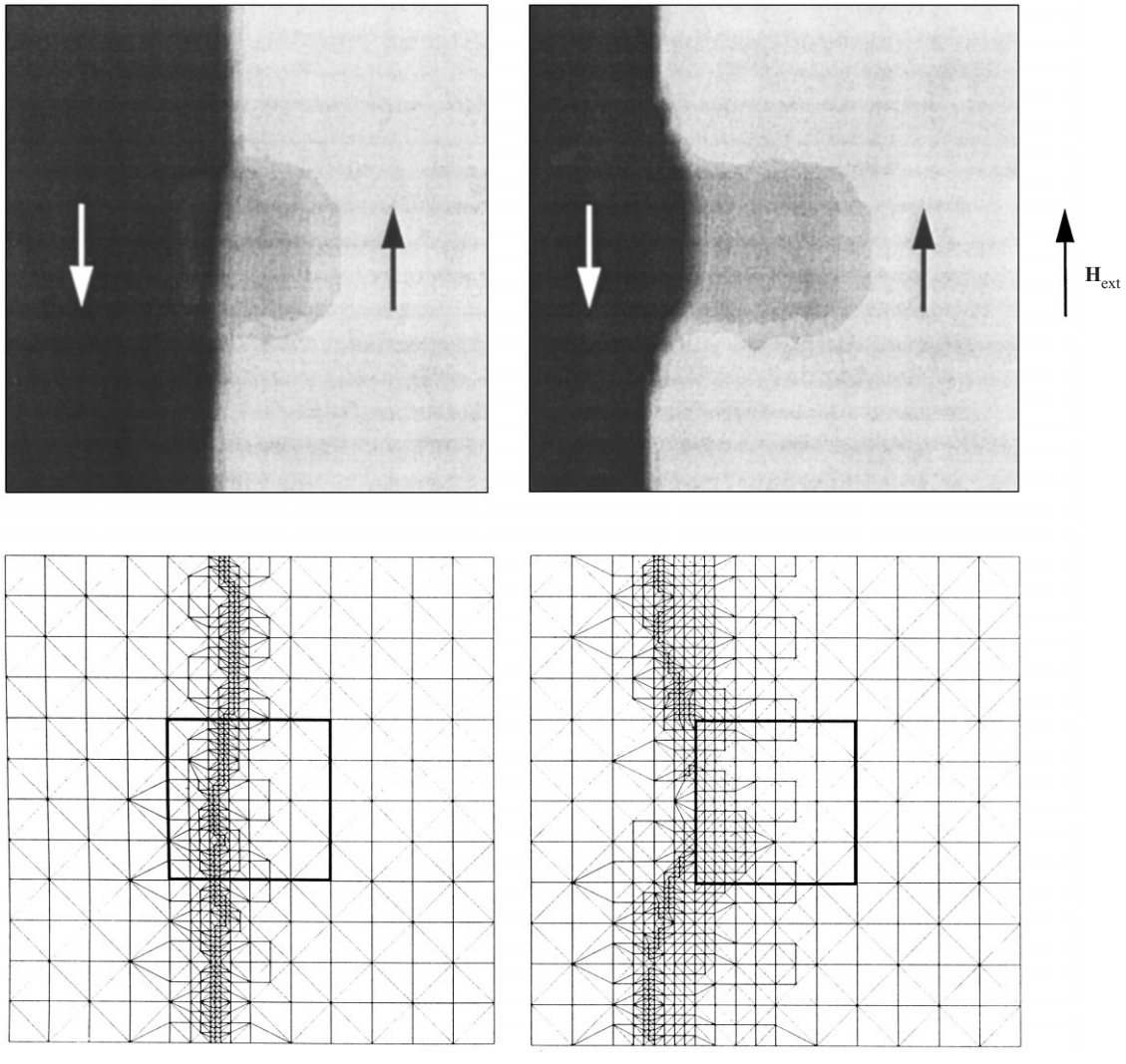

Figure 6
Adaptive mesh refinement: magnetization distribution and corresponding finite element mesh during the simulation of domain wall motion. The wall becomes pinned at the grain boundary of a misoriented grain.

pinned owing to a reduction in the exchange and anistropy energy stored in the wall.

7. Summary

Micromagnetism treats magnetic material as classical continuous media, described by appropriate differential equations governing their static and dynamic behavior. The numerical solution of the governing equations can be effectively performed using finite element and related methods which easily handle complex microstructures. Finite element techniques for an effective solution of the basic static and dynamic equations were compared. These include various methods for treating the so-called open boundary problem in magnetostatic field calculation and discretization schemes that allow sparse matrix methods for the time integration of the equation of motion.

Finite element simulations successfully predict the influence of microstructural features like grain size, particle shape, and edge irregularities on the magnetic properties. Adaptive refinement and coarsening of the mesh controls the discretization error and provides optimal grids for micromagnetic finite element simulation of magnetization processes in longitudinal thin film media, vortex formation in soft magnetic thin films, and of domain wall motion in hard magnetic platelets.

See also: Micromagnetics: Basic Principles

Bibliography

Aharoni A 1996 *Introduction to the Theory of Ferromagnetism*. Clarendon Press, Oxford

Bagnérés-Viallix A, Baras P, Albertini J B 1991 2D and 3D calculations of micromagnetic wall structures using finite elements. *IEEE Trans. Magn.* **27**, 3819–21

Bey J 1995 Tetrahedral grid refinement. *Computing* **55**, 355–78

Brown Jr. W F 1963 *Micromagnetics*. Wiley Interscience, New York

Brunotte X, Meunier G, Imhoff J F 1992 Finite element modeling of unbounded problems using transformations: Rigourous, powerful and easy solutions. *IEEE Trans. Magn.* **28**, 1663–6

Chen Q, Conrad A 1997 A review of finite element open boundary techniques for static and quasi-static electromagnetic field problems. *IEEE Trans. Magn.* **33**, 663–76

Demerdash N A, Wang R 1990 Theoretical and numerical difficulties in 3D vector potential methods in finite element magnetostatic computations. *IEEE Trans. Magn.* **26**, 1656–8

Fischer R, Kronmüller H 1998 Importance of ideal grain boundaries of high remanent composite permanent magnets. *J. Appl. Phys.* **83**, 3271–5

Fredkin D R, Koehler T R 1990 Hybrid method for computing demagnetizing fields. *IEEE Trans. Magn.* **26**, 415–17

Gardiner C W 1985 *Handbook of Stochastic Methods*. Springer, Berlin

Gilbert T L 1955 A Lagrangian formulation of gyromagnetic equation of the magnetization field. *Phys. Rev.* **100**, 1243

Gill P E, Murray W, Wright M H 1993 *Practical Optimization*. Academic Press, London

Hertel R, Kronmüller H 1998 Adaptive finite element mesh refinement techniques in three-dimensional micromagnetic modeling. *IEEE Trans. Magn.* **34**, 3922–30

Hindmarsh A C, Petzold L R 1995 Algorithms and software for ordinary differential equations. Part II: Higher-order methods and software packages. *Comput. Phys.* **9**, 148–55

Khebir A, Kouki A B, Mittra R 1990 Asymptotic boundary for finite element analysis of three-dimensional transmission line discontinuities. *IEEE Trans. Microwave Theory Techniques* **38**, 1427–31

Koehler T R 1997 Hybrid Fem-Bem method for fast micromagnetic calculations. *Physica B* **233**, 302–7

Penman J, Grieve M D 1987 Self adaptive mesh generation technique for the finite element method. *IEEE Proc. A* **134**, 634–50

Preparata F P 1985 *Computational Geometry*. Springer, New York

Ridley P H W, Roberts G W, Wongsam M A, Chantrell R W 1999 Finite element modelling of nanoelements. *J. Magn. Magn. Mater.* **193**, 423–6

Scholz W, Schrefl T, Fidler J 1999 Mesh refinement in FE-micromagnetics for multidomain $Nd_2Fe_{14}B$ particles. *J. Magn. Magn. Mater.* **196–7**, 933–4

Schrefl T, Fidler J 1998 Modelling of Exchange-spring Permanent Magnets. *J. Magn. Magn. Mater.* **177**, 970–5

Schrefl T, Fidler J, Kirk K J, Chapman J N 1999 Simulation of magnetization reversal in polycrystalline Co elements. *J. Appl. Phys.* **85**, 6169–71

Silvester P P, Ferrari R 1983 *Finite Elements for Electrical Engineers*. Cambridge University Press, Cambridge

Süß D, Schrefl T, Fidler J, Chapman J N 1999 Micromagnetic simulation of the long-range interaction between NiFe nanoelements using BE-method. *J. Magn. Magn. Mater.* **196–7**, 617–19

Tako K M, Schrefl T, Wongsam M A, Chantrell R W 1997 Finite element micromagnetic simulations with adaptive mesh refinement. *J. App. Phys.* **81**, 4082–4

Yang B, Fredkin D R 1996 Dynamical micromagnetics of a ferromagnetic particle – Numerical studies. *J. Appl. Phys.* **79**, 5755–7

Yang B, Fredkin D R 1998 Dynamic micromagnetics by the finite element method. *IEEE Trans. Magn.* **33**, 3842–52

R. W. Chantrell, J. Fidler, T. Schrefl,
and M. Wongsam

Encyclopedia of Materials: Science and Technology
ISBN: 0-08-0431526
pp. 5651–5661